



**HAL**  
open science

## Vortex shedding from tandem cylinders

Md. Mahbub Alam, Mehdi Elimer, Longjun Lang, David Lo Jacono, C. W. Wong

► **To cite this version:**

Md. Mahbub Alam, Mehdi Elimer, Longjun Lang, David Lo Jacono, C. W. Wong. Vortex shedding from tandem cylinders. *Experiments in Fluids*, 2018, 59 (3), pp.60. 10.1007/s00348-018-2501-8 . hal-01730852

**HAL Id: hal-01730852**

**<https://hal.science/hal-01730852v1>**

Submitted on 14 Mar 2018

**HAL** is a multi-disciplinary open access archive for the deposit and dissemination of scientific research documents, whether they are published or not. The documents may come from teaching and research institutions in France or abroad, or from public or private research centers.

L'archive ouverte pluridisciplinaire **HAL**, est destinée au dépôt et à la diffusion de documents scientifiques de niveau recherche, publiés ou non, émanant des établissements d'enseignement et de recherche français ou étrangers, des laboratoires publics ou privés.




## Open Archive TOULOUSE Archive Ouverte (OATAO)

OATAO is an open access repository that collects the work of Toulouse researchers and makes it freely available over the web where possible.


This is an author-deposited version published in : <http://oatao.univ-toulouse.fr/>  
Eprints ID : 19633

**To link to this article** : DOI : 10.1007/s00348-018-2501-8  
URL : <http://dx.doi.org/10.1007/s00348-018-2501-8>

**To cite this version:** Alam, Md. Mahbub and Elimer, Mehdi and Longjun, Wang and Lo Jacono, David  and Wong, CW *Vortex shedding from tandem cylinders*. (2018) *Experiments in Fluids*. pp. 1-17. ISSN 0723-4864

Any correspondence concerning this service should be sent to the repository administrator: [staff-oatao@listes-diff.inp-toulouse.fr](mailto:staff-oatao@listes-diff.inp-toulouse.fr)

# Vortex shedding from tandem cylinders

Md. Mahbub Alam<sup>1</sup>  · Mehdi Elhimer<sup>1</sup> · Longjun Wang<sup>1</sup> · David Lo Jacono<sup>2</sup> · C. W. Wong<sup>1</sup>

## Abstract

An experimental investigation is conducted on the flow around tandem cylinders for ranges of diameter ratio  $d/D=0.25-1.0$ , spacing ratio  $L/d=5.5-20$ , and Reynolds number  $Re=0.8 \times 10^4-2.42 \times 10^4$ , where  $d$  and  $D$  are the diameters of the upstream and downstream cylinders, respectively,  $L$  is the distance from the upstream cylinder center to the forward stagnation point of the downstream one. The focus is given on examining the effects of  $d/D$ ,  $L/d$  and  $Re$  on Strouhal number  $St$ , flow structures and fluid forces measured using hotwire, particle image velocimetry (PIV) and load cell measurement techniques, respectively. Changes in  $d/D$  and  $L/d$  in the ranges examined lead to five flow regimes, namely lock-in, intermittent lock-in, no lock-in, subharmonic lock-in and shear-layer reattachment regimes. Time-mean drag coefficient ( $C_D$ ) and fluctuating drag and lift coefficients ( $C'_D$  and  $C'_L$ ) are more sensitive to  $L/d$  than  $d/D$ . The scenario is opposite for  $St$  where  $d/D$  is more prominent than  $L/d$  to change the  $St$ . The detailed facet of the dependence on  $d/D$  and  $L/d$  of  $C_D$ ,  $C'_D$ ,  $C'_L$  and  $St$  is discussed based on shear-layer velocity, approaching velocity, vortex formation length, and wake width.

## 1 Introduction

Extensive studies have been carried out to investigate the flow around and forces on circular cylinders. This is important in many engineering applications, such as high-rise buildings or skyscrapers, chimney stacks, overhead power-line bundles, submarine communication system, oil pipeline, and tube bundles in heat exchangers. The tandem cylinders in cross-flow have particularly attracted considerable attention. This is not only because the knowledge of the flow around tandem circular cylinders is fundamental to understand the flow around multiple cylinders in complex arrangements but also because the flow interference between the tandem cylinders causes wake-induced vibrations. This flow configuration is shown in Fig. 1 with the relevant geometrical parameters. The nature of the flow around tandem cylinders is highly dependent on the spacing between the cylinders (Alam et al. 2003; Sumner et al. 2010; Mahir and

Altac 2008; Alam 2016), Reynolds number (Igarashi 1984; Alam 2014) and the ratio of the cylinder diameters (Mavridou and Bouris 2012; Qin et al. 2017; Wang et al. 2017).

Zdravkovich (1977) classified the flow around tandem identical diameter ( $d/D=1.0$ ) cylinders into three major regimes (extended body, reattachment, and coshedding), where  $d$  and  $D$  are the upstream and downstream cylinder diameters, respectively (Fig. 2). The extended body regime occurs at  $0.5 < L/d < 1.0$  ( $L$  is the distance between the center of the upstream cylinder and the forward stagnation point of the downstream cylinder), where the two cylinders are so close to each other that the free shear layers separating from the upstream cylinder (UC) overshoot the downstream cylinder (DC), and the flow in the gap between the cylinders is almost stagnant (Fig. 2a). The reattachment regime prevails at  $1.0 < L/d < 3.5$ , where the shear layers separating from the UC reattach on the DC, while the flow velocity in the gap is not stagnant but very small (Fig. 2b). The coshedding regime appears at  $L/d > 3.5$ , where the shear layers roll up alternately in the gap between the cylinders, inducing a relatively large flow velocity in the gap (Fig. 2d). There is a transition  $L/d$  range between the reattachment and coshedding regimes, where both reattachment and coshedding flows appear intermittently, switching from one to the other (Fig. 2c). The transition  $L/d$  is also called the critical or bistable flow spacing.

---

✉ Md. Mahbub Alam  
alam28@yahoo.com; alam@hit.edu.cn

<sup>1</sup> Shenzhen Graduate School, Institute for Turbulence-Noise-Vibration Interaction and Control, Harbin Institute of Technology, Shenzhen 518055, China

<sup>2</sup> Institut de Mécanique des Fluides de Toulouse (IMFT), Université de Toulouse, CNRS, INPT, UPS, Toulouse, France

**Fig. 1** Geometrical parameters and definitions of symbols for tow tandem cylinders

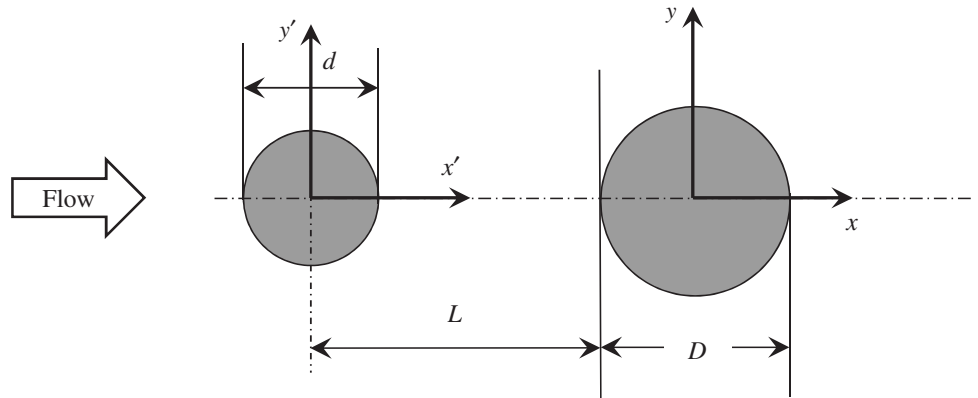
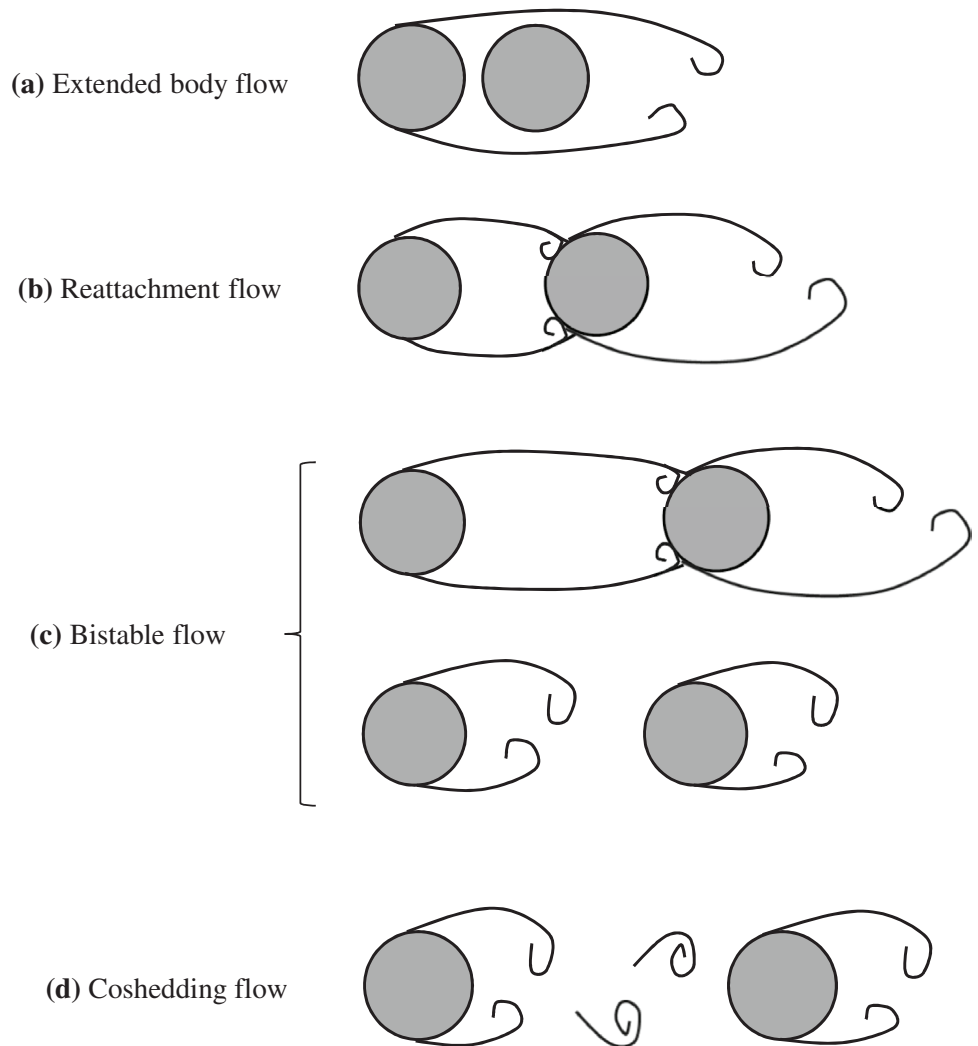


**Fig. 2** Schematics of the possible flow structures for two tandem cylinders of equal diameters



In the coshedding regime, the two cylinders of  $d/D=1.0$  shed vortices separately at the same frequency (e.g., Igarashi 1981, 1984; Alam et al. 2003; Alam 2016; Wang et al. 2017). Alam and Sakamoto (2005) identified that, for a given  $DC$  in the coshedding regime, a change in the  $UC$  cross-sections of the same characteristic width results

in a difference in the shedding frequency of the  $UC$ , and the frequency of vortex shedding from the  $DC$  modifies accordingly, adjusting itself to that of the  $UC$ . This phenomenon is called "lock-in" (Sakamoto and Haniu 1988; Alam and Sakamoto 2005). Alam et al. (2003) measured

$St$  and showed that the two cylinders shed vortices at the same frequency at least up to  $L/d = 10$ .

Most of the studies in the literature have been conducted for  $d/D = 1.0$ . Knowledge of the effect of  $d/D$  on the flow around the cylinders is scarce. In engineering applications, however, the two interacting bluff bodies may have different sizes ( $d/D \neq 1.0$ ). The difference in the cylinder size induces differences in wake sizes, vortex sizes and vortex shedding frequencies of the two cylinders, further aggravating the complexity of the fluid dynamics. It is not clear how  $d/D \neq 1.0$  affects the fluid dynamics, in comparison with the case of  $d/D = 1.0$ . More specifically, for example, how a decrease in  $d/D$  from 1.0 will affect flow regimes, forces, and Strouhal numbers of the DC, for a given  $L/d$ . Only a few studies have however been dedicated to the case of  $d/D \neq 1.0$ . The use of a small UC to decrease the drag on a larger DC was reported in several studies (Lee et al. 2004; Lesage and Gartshore 1987; Prasad and Williamson 1997). These works highlighted the occurrence of reattachment and coshedding modes depending on  $L/d$ , with a bistable flow at the transition  $L/d$ . Significant drag reduction was achieved in the reattachment regime because of the low pressure on the front surface of the DC due to a cavity flow formed in the gap. The largest drag reduction was identified for a small  $d/D$ , for instance, a 25% reduction in time-mean drag occurring for  $d/D = 0.233$  (Lee et al. 2004).

Hiwada et al. (1979) considered a smaller UC as a turbulence generator for increasing the heat and mass transfer in the wake of the DC. They for  $d/D = 0.13$ – $0.52$  investigated how the turbulence induced by the UC affects the local heat transfer around the DC. The turbulence produced by the UC alters the boundary layer separation of the DC, hence increased heat transfer. Zhao et al. (2005) conducted a numerical simulation of the wake of two different cylinders with  $d/D = 0.25$  and found that the gap between the cylinders had a significant effect on the forces on the DC. A decrease in drag coefficient was observed when the gap distance was increased from  $0.05D$  to  $1.0D$ . Igarashi (1982) identified reattachment, bistable and coshedding flows for  $d/D = 1.47$  in a similar fashion to those for  $d/D = 1.0$ . The bistable flow regime was shorter for  $d/D = 1.47$  than for  $d/D = 1.0$ .

Baxendale et al. (1986) investigated the effect of  $d/D$  ( $= 0.422$ – $0.571$ ) on the vortex shedding from the DC for  $L/d = 3.3$  and  $3.9$ ,  $Re = 1.55 \times 10^4$  and  $4.92 \times 10^4$ . When  $d/D \approx 0.5$ , the vortex shedding frequency of the DC was locked-in to the half of that of the UC. This phenomenon, called “subharmonic lock-in” here, was also observed in the case of a single cylinder subjected to a pulsating flow. In this flow, the upstream velocity is unsteady and varies periodically with a “pulsating” frequency. This frequency is in general different from the Strouhal frequency (vortex shedding frequency) of the cylinder. When the pulsating frequency is close to twice the Strouhal frequency of the DC,

the vortex shedding frequency remains locked-on to half the pulsating frequency (Barnes and Grant 1983; Konstantinidis et al. 2003; Konstantinidis and Balabani 2008). In the case of a pulsating flow, Konstantinidis et al. (2003) observed that the DC wake shares many characteristics with that of a transversely or inline oscillating cylinder. These include the shortening of the recirculation bubble and vortex formation length. The shortening is shown to be the largest when the subharmonic lock-in occurs.

Alam and Zhou (2008) at  $Re = 450$  and  $2.72 \times 10^4$  for a fixed  $L/d = 5.5$  studied the effect of  $d/D$  ( $= 0.24$ – $1.0$ ) on the vortex shedding frequencies from both cylinders as well as the flow structure and the forces on the DC. Based on the power spectral analysis results of hotwire-measured streamwise velocities, one and two Strouhal peaks were reported for the UC and DC, respectively. For the DC, the first peak frequency was equal to that of the UC, the second peak frequency was always lower and ascribed to the vortex shedding for the DC. The UC wake narrows with decreasing  $d/D$  (Fig. 3a–e). Through wavelet analysis and visualizations, it was shown that the vortex shedding frequency from the DC is intermittently locked-in to that of the UC (Fig. 3f, g). This phenomenon was hence termed “intermittent lock-in” (Alam and Zhou 2008). With  $d/D$  decreasing, the Strouhal numbers of the UC and DC varied oppositely, declining and growing, respectively. Particularly at  $d/D = 0.6$ , the UC shedding frequency was exactly twice the DC, which was a subharmonic lock-in (Alam and Zhou 2008). Note that their work was limited to  $L/d = 5.5$ ,  $Re = 450$  and  $2.72 \times 10^4$  and  $d/D = 0.24$ ,  $0.4$ ,  $0.6$ ,  $0.5$  and  $1.0$ . The resolution in  $d/D$  seems coarse to provide more details on the subharmonic lock-in. Their constrained initial conditions and observations lead to a very important question: are the lock-in and subharmonic lock-in dependent on  $L/d$ ,  $d/D$  and  $Re$ ? Furthermore, investigations for a large  $L/d$  (e.g.  $> 7$ ) are scarce.

The present work aims to perform an investigation of tandem cylinders ( $d/D = 0.25$ ,  $0.5$ ,  $0.55$ ,  $0.6$ ,  $0.65$ ,  $0.7$ ,  $0.8$  and  $1.0$ ) for large  $L/d = 5.5$ – $20$  and  $Re = 0.8 \times 10^4$ – $2.42 \times 10^4$ , examining the influence of  $L/d$  and  $Re$  on the vortex shedding frequency, flow structure, fluid forces, and subharmonic lock-in. The  $d$  is varied while  $D$  is kept fixed, so that  $d/D$  varies from  $0.25$  to  $1.0$ . Hotwire, load cell, and particle image velocimetry (PIV) measurement techniques are employed to measure shedding frequency, forces, and flow field, respectively.

## 2 Experimental setup

### 2.1 Wind tunnel and cylinder models

Experiments were performed in a wind tunnel with a 2.0-m-long test section of 0.3 m in width and 0.3 m in

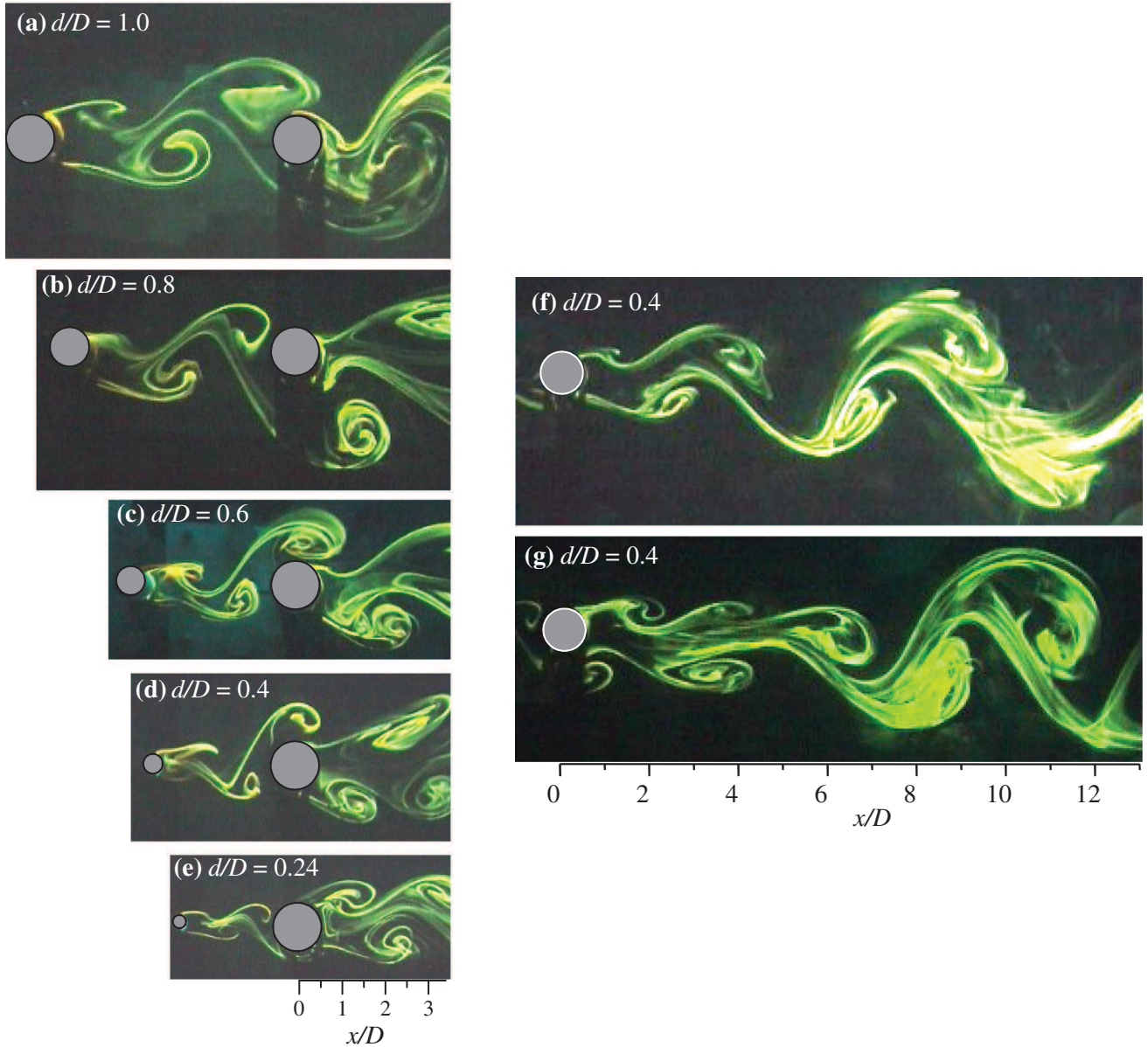


**Fig. 3** a–e Photographs of the gap flow with change in  $d/D$  at  $L/d=5.5$ . f, g Distinct flow structures at different instants behind the downstream cylinder at  $d/D=0.4$ , showing intermittent lock-in.

Low-frequency vortices generated by the downstream cylinder in (f) and high-frequency vortices generated by the downstream cylinder ( $x/D < 5$ ) in (g). Alam and Zhou (2008)

height. The free stream velocity was  $U_\infty = 6\text{--}18$  m/s, corresponding to  $Re (\equiv U_\infty D/\nu) = 0.8 \times 10^4\text{--}2.42 \times 10^4$ , where  $\nu$  is the kinematic viscosity of air. The turbulence intensity was less than 0.4% in this  $U_\infty$  range. The  $U_\infty$  was measured using a pitot-static tube connected to a micro-manometer (Furness FCO510, 0–20 mm H<sub>2</sub>O, 0–18 m/s), with an uncertainty of less than 2%. The downstream cylinder diameter  $D$  was fixed at 20 mm, while the upstream cylinder diameter  $d$  was changed as  $d = 5, 10, 11, 12, 13, 14, 16,$  and 20 mm, resulting in diameter ratios  $d/D = 0.25, 0.5, 0.55, 0.6, 0.65, 0.7, 0.8$  and 1.0, respectively. The  $L/d$  was systematically

varied as 5.5, 10, 15 and 20. The cylinders were spanned the full width of the working section, resulting in a maximum blockage ratio of 6.7% based on  $D$  and a minimum aspect ratio (AR) of 15. Given that the aspect ratio is relatively high and force measurement is carried out by a load cell mounted at one end of the cylinder, no end plates were used. The minimum distance between the center of the downstream cylinder to the end of the test section is 960 mm ( $48D$ ) in the case of  $(d/D, L/d) = (1.0, 15)$ . This distance is long enough for the wake to develop (Lau et al. 2004; Assi et al. 2010). A schematic diagram of the cylinder arrangement is given in



Fig. 4. Two Cartesian coordinate systems are employed such that the origins are at the centers of the UC and DC, with  $x$ - and  $y$ -axis along the streamwise and lateral directions, respectively (Fig. 4b).

## 2.2 Shedding frequency measurement

Two single tungsten hotwires (HT1 and HT2), placed in the gap ( $x'/d=2.0$ ,  $y'/d = -1.0$ ) between the cylinders and behind (at  $x/D=4.0$ ,  $y/D=1.0$ ) the DC, respectively, were used to measure the streamwise velocity fluctuations  $u_1$  and  $u_2$  (Fig. 4a, b). The hotwires (Pt-10% Rh, Dantec 55P01) were each  $0.5 \mu\text{m}$  in diameter and  $1.25 \text{ mm}$  in length. The hotwire probe holder was placed perpendicular to the wake-centerline plane to minimize the disturbance to the flow (Alam and Zhou 2007; Alam et al. 2010). The signals were captured at a sampling frequency  $1.5 \text{ kHz}$  over a sampling duration of  $30 \text{ s}$  (Wang et al. 2017). The power spectral density functions  $E_{u1}$  and  $E_{u2}$  of  $u_1$  and  $u_2$  were calculated using fast Fourier transform (FFT) from which

vortex shedding frequencies were extracted. A 16-channel analogue/digital board was used to acquire the hotwire signals. A low-pass filtering (cut-off frequency  $1.0 \text{ kHz}$ ) and amplification were applied to the analogue signals before digitization. The power spectral density functions were determined based on the average of 10 runs, each with  $2^{12}$  samples. The frequency resolution in the power spectra was  $0.36 \text{ Hz}$ , resulting in an uncertainty of approximately  $\pm 3\%$  in the estimate of  $St$  in an isolated single cylinder wake.

## 2.3 Flow field measurements

Particle image velocimetry (PIV) and smoke visualization measurements were also conducted in the same wind tunnel. A Dantec high-frequency PIV system (Litron LDY 304-PIV, Nd: YLF, maximum triggering frequency is  $727 \text{ Hz}$  for double frames) was used to measure the flow velocities in the gap and near wake in the  $(x, y)$  plane. The cylinder surface and the tunnel wall hit by the laser sheet were painted black to minimize reflection noises. The flow was seeded by

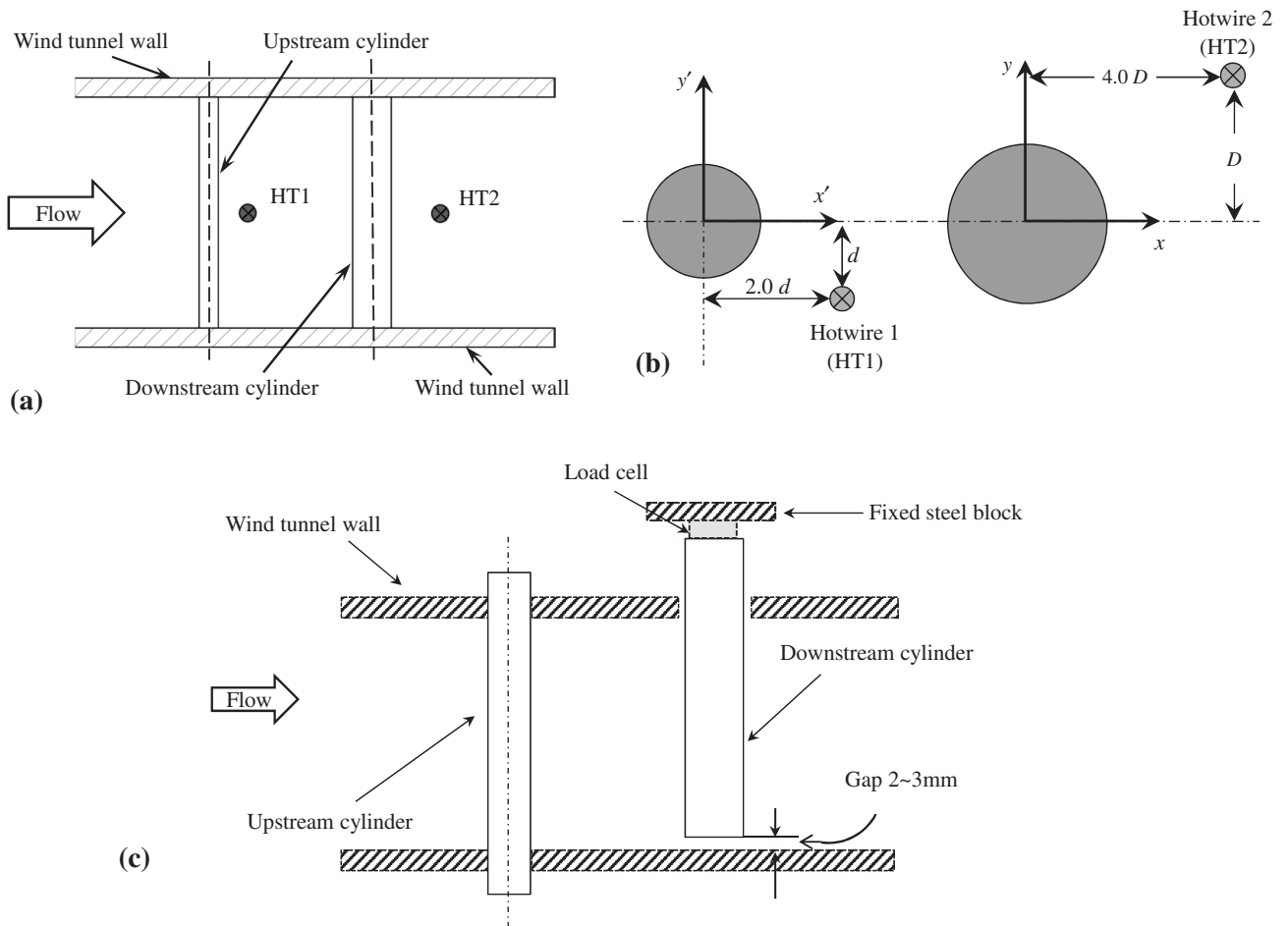


Fig. 4 a Sketches of the cylinders and positions of the hotwires in wind tunnel. b Side view showing the positions of the hotwires. c Sketch of the force measurement setup

particles, generated from paraffin oil using a TSI 9307-6 particles generator, with a particle size of about 1.0  $\mu\text{m}$  in diameter. Flow illumination was provided by two pulse laser sources of a 527 nm wavelength, each with a maximum energy output of 30 mJ per pulse. One CCD camera (PhantomV641, double-frame, with a resolution of  $2560 \times 1600$  pixels) was used to capture particle images. A Dantec timer box 80N77 was used to synchronize laser pulses and particle images. In image processing, an adaptive PIV method with an interrogation window of  $32 \times 32$  pixels was used with 50% overlap in each direction. There were 800 images captured for each ( $d/D$ ,  $L/d$ ) to estimate time-mean streamwise velocity ( $\bar{u}$ ) and r.m.s. velocity ( $u_{\text{rms}}$ ). The progressively  $\bar{u}$  and  $u_{\text{rms}}$  at the point corresponding to the shear layer roll-up position, where  $u_{\text{rms}}$  is maximum, were confirmed to approach their asymptotic values when the number of images reached 500 (Alam et al. 2011). The  $\bar{u}$  and  $u_{\text{rms}}$  at a given position are obtained as  $\bar{u} = \frac{1}{N} \sum_{i=1}^N u_i$  and  $u_{\text{rms}} = \sqrt{\frac{1}{N} \sum_{i=1}^N (u_i - \bar{u})^2}$ , respectively, where  $N$  is the number of data samples and  $u_i$  is the velocity value for a sample  $i$ . The normalized  $\bar{u}$  and  $u_{\text{rms}}$  are represented as  $\bar{u}^* = \bar{u}/U_\infty$  and  $u_{\text{rms}}^* = u_{\text{rms}}/U_\infty$ , respectively. In this paper, the asterisk denotes normalization by  $D$  and/or  $U_\infty$ . In the uncertainty measurements of mean and r.m.s. velocities, 2000 images (samples) were captured for the single cylinder. The progressive averaged and r.m.s. values of the streamwise velocity at the point corresponding to the shear-layer rolling position (maximum  $u_{\text{rms}}^*$ ) indicated that the  $\bar{u}^*$  and  $u_{\text{rms}}^*$  approached their asymptotic values when the sample size is about 500. The moving averaged data with a running sample of 500 showed an uncertainty of  $\pm 2.8\%$  for  $\bar{u}^*$  and  $\pm 3.3\%$  for  $u_{\text{rms}}^*$ .

## 2.4 Force measurements

A three-component load cell (Minebea MX020-10N-S02, 10N) was installed at the upper end of the DC to measure the fluid forces. To avoid the gravity force, the cylinders are installed vertically so that there is a 2–3 mm gap between the DC edge and the wind tunnel wall (Fig. 4c). The load cell was bolted tightly on a stainless steel block (Fig. 4c). To avoid the effect of wind tunnel vibration on the measurements, the load cell holder was mounted on an external rigid frame detached from the wind tunnel. The external frame was made of aluminium bars, with four (two on each side of the tunnel) supporting legs fixed on the ground. The rigidity of the frame was further increased by adding cross bars on the supporting legs. Before conducting extensive force measurements by the load cell system, the signal of the lift force on the cylinder mounted on the frame was captured and its power spectrum was made. The power spectrum displayed a sharp peak corresponding to the vortex shedding frequency;

no other frequencies were detected, confirming that vibration of the external frame is negligible.

The load cell measures instantaneous integral fluid forces acting on the length of the cylinder exposed in the wind tunnel. The load cell was calibrated using dead weights before the measurement campaign. The time-mean drag coefficient  $C_D$ , fluctuating drag coefficient  $C'_D$ , and fluctuating lift coefficient  $C'_L$  were estimated as  $C_D = \frac{F_D}{0.5\rho U_\infty^2 L_0 D}$ ,  $C'_D = \frac{F'_D}{0.5\rho U_\infty^2 L_0 D}$  and  $C'_L = \frac{F'_L}{0.5\rho U_\infty^2 L_0 D}$ , where  $F_D$ ,  $F'_D$  and  $F'_L$  are the time-averaged drag, fluctuating (r.m.s.) drag, and fluctuating (r.m.s.) lift forces, respectively, on the length  $L_0$  of the cylinder exposed in the wind tunnel. To estimate uncertainties in the measurement of  $C_D$ , the load cell signal was captured for about 5 min, corresponding to 450,000 samples for a single cylinder at  $Re = 1.6 \times 10^4$ . Then, the moving average of the data series was conducted with a running sample size of 45,000 that was the sample size for the estimate of  $C_D$ . The distribution of the 405,000 sample averages ( $= 450,000 - 45,000$ ) was obtained and the corresponding standard deviation ( $\sigma$ ) was approximately 1.3% of the mean value. The value of  $2\sigma$ , which corresponds to a 95% confidence level, was taken as the measurement uncertainty, i.e., the uncertainty of the data from the mean is  $\pm 2.6\%$  for  $C_D$ . The same technique was employed to estimate the uncertainties in  $C'_D$ ,  $C'_L$ , and  $U_\infty$ , which were  $\pm 3.7$ ,  $\pm 3.1$ , and  $\pm 2\%$ , respectively.

## 2.5 Force and Strouhal number measurement validations

Before conducting extensive measurements for the two-cylinder case, we measured forces and Strouhal number of a single isolated cylinder to validate the measurements from the load cell and hotwire anemometers. Norberg (1994) presented a compilation of  $St$  as a function of  $Re$  from selected experiments and numerical simulations. A comparison is made in Table 1 of our Strouhal number  $St (= f_v D/U_\infty)$  results with those from Norberg's compilation, where  $f_v$  is the vortex shedding frequency. The present results are slightly higher than Norberg's (1994), both results having the same trend, decreasing with  $Re$ . The higher values

**Table 1** Comparison of  $St$  between the present study and Norberg's (1994)

$Re$	$St$	
	Present	Norberg (1994)
$0.8 \times 10^4$	0.210	0.205
$1.6 \times 10^4$	0.208	0.199
$2.24 \times 10^4$	0.206	0.194



obtained presently can be attributed to the higher turbulence intensity ( $\approx 0.4\%$ ) in the present experiment compared to that ( $< 0.06\%$ ) in Norberg's.

Similarly, Table 2 compares  $C_D$ ,  $C'_D$ , and  $C'_L$  with those reported in West and Apelt (1993, 1997) for the same aspect ratio and similar blockage ratio (6%) at  $Re = 2.42 \times 10^4$ . The present  $C_D$  and  $C'_L$  are lower than West and Apelt's, both by 0.03, while the present  $C'_D$  is higher by 0.024. The difference, albeit small, could be attributed to the experimental uncertainties, experimental conditions, and measurement techniques. In the experiment by West and Apelt, end plates

**Table 2** Comparison of force coefficients between the present study and West and Apelt's (1993, 1997) at  $Re = 2.42 \times 10^4$

Force coefficients	West and Apelt	Present
$C_D$	1.14	1.11
$C'_D$	0.064	0.088
$C'_L$	0.342	0.310

were used, the cylinder had an aspect ratio of 10, and forces were measured using pressure taps on the circumference of the cylinder. A fairly good agreement is found between the two sets of results.

## 3 Results and discussion

### 3.1 Vortex shedding frequencies

Figures 5, 6 and 7 show the power spectral density functions  $E_{u1}$  (dotted red line) and  $E_{u2}$  (solid black line) at  $d/D = 1.0$ , 0.8, 0.65, 0.6 and 0.25 for  $L/d = 5.5-20$  and  $Re = 0.8 \times 10^4$ ,  $1.61 \times 10^4$ , and  $2.42 \times 10^4$ . As mentioned in Sect. 2, the  $E_{u1}$  and  $E_{u2}$  provide information on the shedding frequencies of the UC and DC, respectively. The Fourier frequency in the horizontal axis is normalized based on  $U_\infty$  and  $D$ . The  $St$  values are marked in the figures. Let us first examine the case of  $d/D = 1.0$  (Fig. 5a, b, c). At  $L/d = 5.5$ , a single pronounced peak emerges in  $E_{u1}$  for all  $Re$ . The corresponding

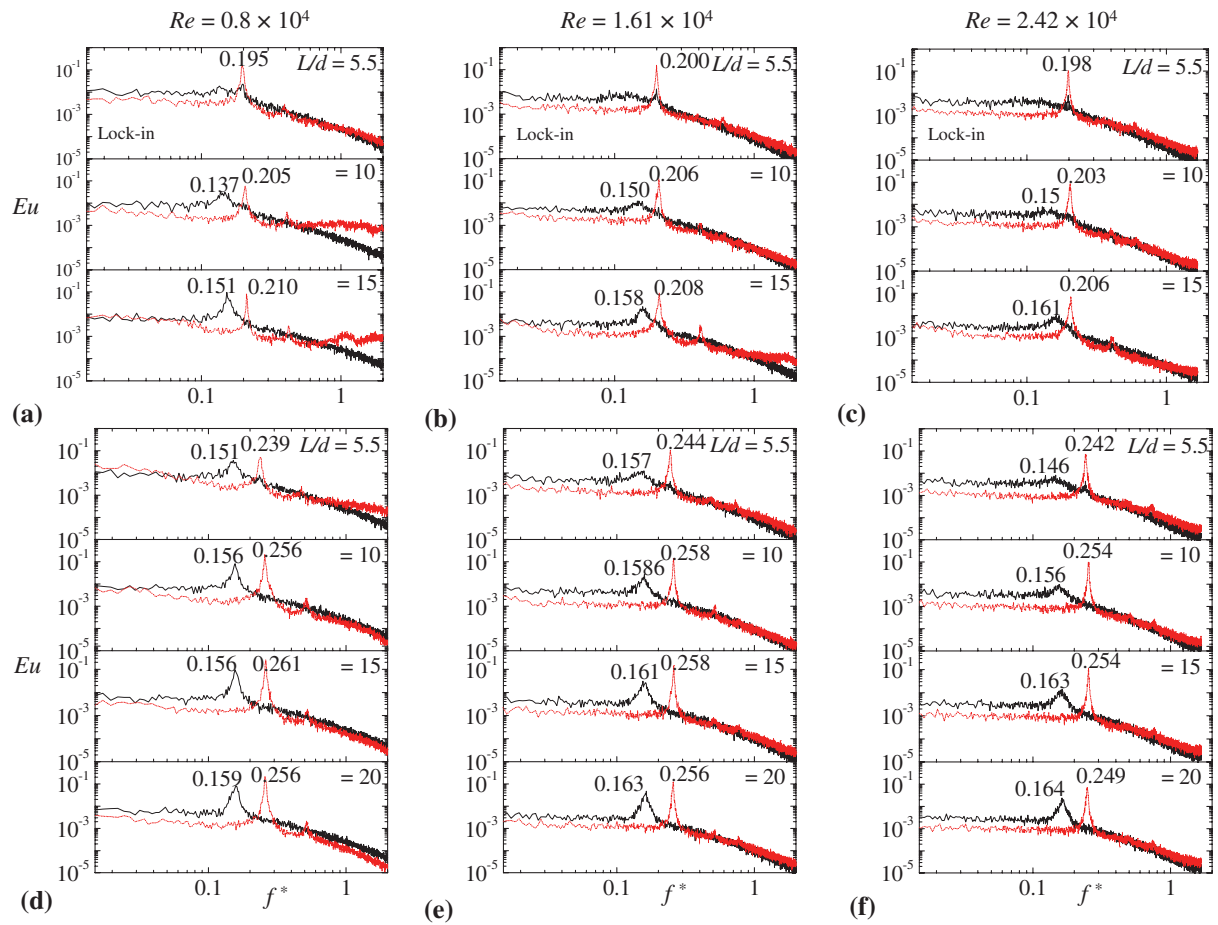


**Fig. 5** The power spectral density functions  $E_{u1}$  (dotted red line, HT1) and  $E_{u2}$  (solid black line, HT2) for various  $Re$  and  $L/d$ . **a-c**  $d/D = 1$ ; **d-f**  $d/D = 0.8$ . First, second and third columns for

$Re = 0.8 \times 10^4$ ,  $1.61 \times 10^4$  and  $2.42 \times 10^4$ , respectively. The horizontal axis is the normalized Fourier frequency  $f^* = fD/U_\infty$ . The  $St$  values, corresponding to the peaks are marked in each power spectrum

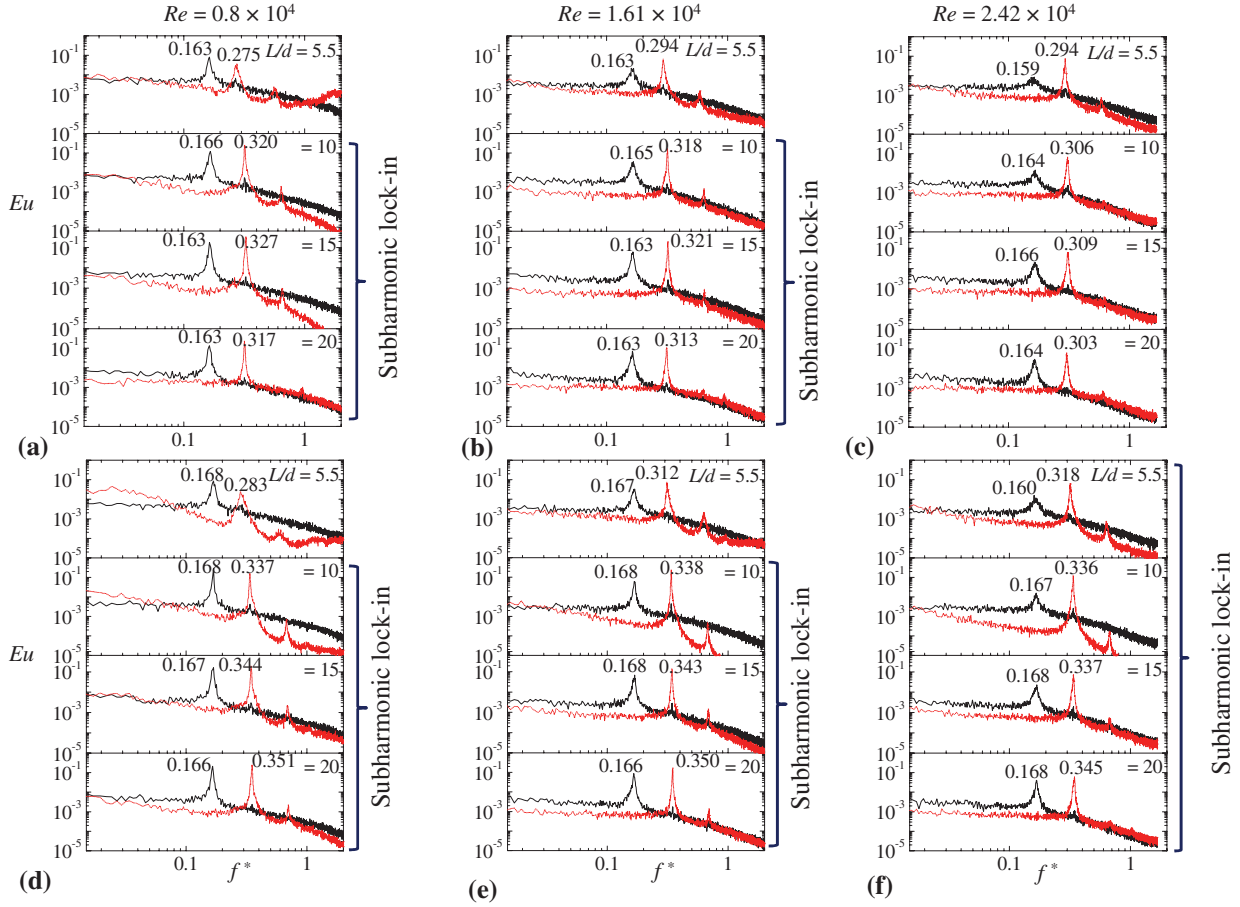


**Fig. 6** The power spectral density functions  $E_{u1}$  (dotted red line) and  $E_{u2}$  (solid black line) for various  $Re$  and  $L/d$ . (a, b, c)  $d/D=0.65$ ; **d-f**  $d/D=0.60$ . First, second and third columns for  $Re=0.8 \times 10^4$ ,

$1.61 \times 10^4$  and  $2.42 \times 10^4$ , respectively. The horizontal axis is the normalized Fourier frequency  $f^* = fD/U_\infty$ . The  $St$  values, corresponding to the peaks, are marked in each power spectrum

$St$  slightly increases with increasing  $L/d$ , regardless of  $Re$ . At the largest  $L/d$  ( $=15$ ) where the UC may not be influenced by the DC, the  $St$  of the UC decays slightly from 0.21 to 0.206 as  $Re$  increases from  $0.8 \times 10^4$  to  $2.42 \times 10^4$ . A single isolated cylinder  $St$  in the subcritical regime is the maximum of 0.212 at  $Re=0.2 \times 10^4$ , decreasing to 0.19 at  $Re=4 \times 10^4$  (Zdravkovich 1997). That is, the decrease in  $St$  of the UC follows that of the single cylinder, the UC behaving like an isolated cylinder at  $L/d=15$ .

For the DC, one peak is identifiable at  $L/d=5.5$ , prevailing at the same frequency as measured for the UC. The occurrence of this peak is ascribed to the lock-in of the DC shedding with the UC (Alam and Zhou 2008). The convective vortices from the UC trigger the vortex shedding from the DC, which results in the lock-in. At  $L/d=10$ , two  $St$ (s) are observed, one is identical to that of the UC, and the other is smaller ( $St=0.137$ – $0.15$ , depending on  $Re$ ), suggesting an intermittent lock-in of the DC shedding with the UC. The duration of the lock-in occurrence is perhaps short, as the associated peak is small. At  $L/d=15$ , only one  $St$  is

identified, nestling at  $St=0.151$ – $0.161$  depending on  $Re$ . The corresponding peak becomes sharper than that at  $L/d=10$ . The lock-in is absent for  $L/d=15$ . The absence of lock-in for a larger  $L/d$  can be explained as that the UC vortices decaying downstream become very weak before reaching the DC, failing to trigger the DC vortex shedding. This observation suggests that there exists a critical spacing beyond which the UC fails to trigger the vortex shedding from the DC.

Now let us see  $St$  characteristics of the two cylinders when  $d/D \neq 1.0$ . Figure 5d–f is for  $d/D=0.8$  at  $Re=0.8 \times 10^4$ ,  $1.61 \times 10^4$ , and  $2.42 \times 10^4$ , respectively. Identified are one single  $St$  for the UC and two  $St$ (s) for the DC at  $L/d=5.5$ . The lower  $St$  peak of the DC is more dominant than the higher. The higher  $St$  of the DC is, however, the same as that of the UC, indicating an intermittent lock-in of the DC vortex shedding to the UC. When the spacing is increased to  $L/d=10$ – $20$ , the higher  $St$  peak for the DC vanishes, where the two cylinders shed vortices individually, no lock-in taking place. Compared to  $d/D=1$  counterparts, (1) the  $St$  of the UC is enlarged at  $d/D=0.8$ ,

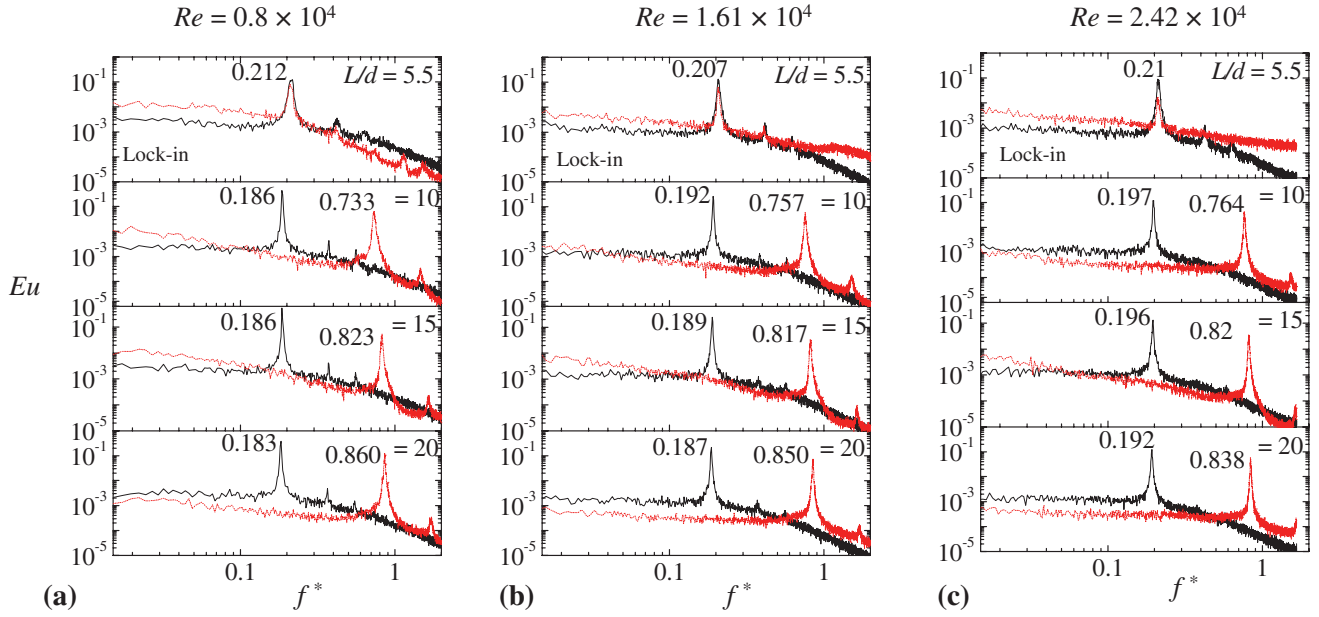


**Fig. 7** The power spectral density functions  $E_{u1}$  (dotted red line) and  $E_{u2}$  (solid black line) for  $d/D=0.25$ . First, second and third columns for  $Re=0.8 \times 10^4$ ,  $1.61 \times 10^4$  and  $2.42 \times 10^4$ , respectively. The hori-

zontal axis is the normalized Fourier frequency  $f^* = fD/U_\infty$ . The  $St$  values, corresponding to the peaks, are marked in each power spectrum

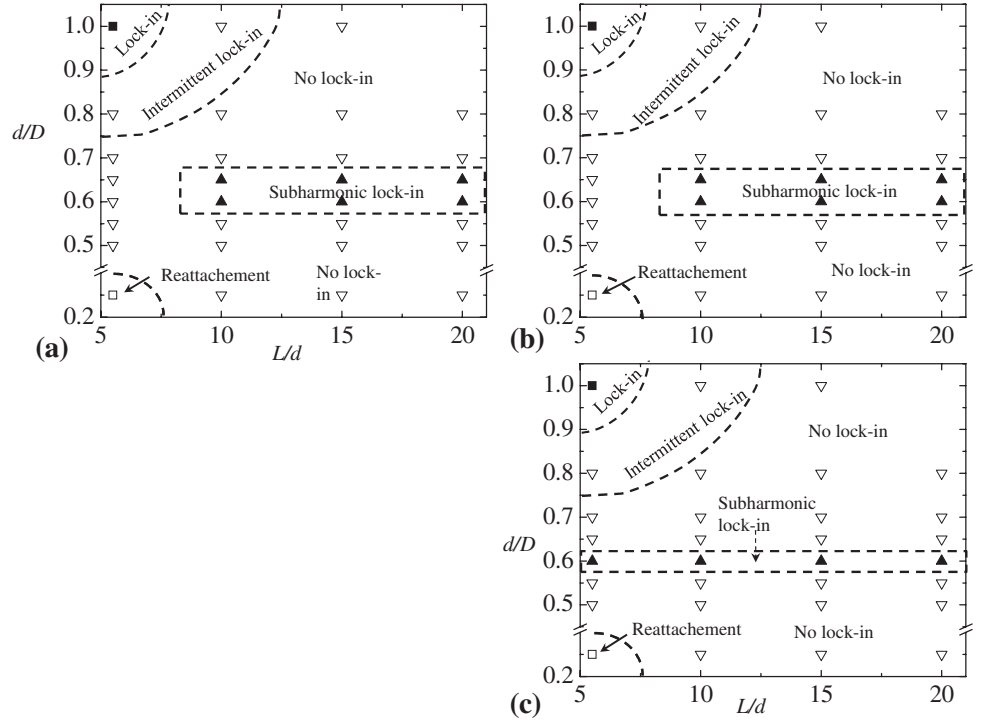
and (2) the peak for the DC is clearer at all  $Re$  and  $L/d$ . One may wonder why  $St$  of the UC at  $d/D=0.8$  is larger than that at  $d/D=1.0$ . Since the UC diameter is now small, i.e.,  $d=0.8D$ , its shedding frequency is higher, given the same incident flow velocity. Power spectral characteristics at  $d/D=0.7$  were similar to those at  $d/D=0.8$ , hence not presented.

The spectral characteristics at  $d/D=0.65$  and  $0.60$  (Fig. 6) bear some distinct features from and some similarities to those at  $d/D=0.8$ . The similarities are that the  $St(s)$  of the two cylinders are different from each other, the UC having a higher  $St$  than the DC. The  $St$  peak of the UC is more pronounced than that at  $d/D=0.8$ . The distinct features here are that, except for  $d/D=0.65$ ,  $Re=2.42 \times 10^4$  (Fig. 6c), (1)  $St$  of the UC jumps between  $L/d=5.5$  and  $10$ , becoming weakly sensitive to a further increase in  $L/d$  ( $=10-20$ ), (2) between the same  $L/d$  ( $=5.5$  and  $10$ ), the jump for the DC is insignificant, and (3)  $St$  of the DC is nearly half ( $=0.48-0.52$ , lying within the uncertainty due to the frequency resolution in power spectra) that of the UC for  $L/d=10-20$ . The observation points to a subharmonic lock-in of the shedding from the two cylinders. For  $d/D=0.65$ ,  $Re=2.42 \times 10^4$ , a jump in  $St$  is absent and the ratio of the  $St$  of the DC to the UC is not half, hence subharmonic lock-in does not occur. The lock-in thus sustains itself for  $d/D=0.65$ ,  $L/d=10-20$ ,  $Re=0.8 \times 10^4-1.61 \times 10^4$ , and for  $d/D=0.65$ ,  $L/d=10-20$ ,  $Re=0.8 \times 10^4-2.42 \times 10^4$ . The subharmonic lock-in was not identified for  $d/D=0.55$  and  $0.50$ , the results are, therefore, not presented here.

A different scenario emerges for  $d/D=0.25$  (Fig. 7). The  $St(s)$  of the two cylinders are identical at  $L/d=5.5$  and different from each other for  $L/d=10-20$ . The physics of the identical  $St$  for  $d/D=0.25$ ,  $L/d=5.5$ , however, differs from that for  $d/D=1.0$  or  $0.8$ ,  $L/d=5.5$ . It was found that the shear layers separating from the UC reattach on the DC for  $d/D=0.25$ ,  $L/d=5.5$ , leading to a reattachment flow. Wang et al. (2017) examined the flow structures for  $d/D=0.2-1.0$  at  $Re=4.27 \times 10^4$ ,  $L/d < 8$  and found that while the critical spacing separating the reattachment and coshedding flows is  $L/d=2.5$  for  $d/D=1.0$ , it grows to  $L/d=6.5$  for  $d/D=0.2$ . They connected the critical  $L/d$  to dependence on  $Re$  of vortex formation length of a single cylinder, given the upstream cylinder behaving almost like an isolated single cylinder. Alam and Zhou (2008), however, obtained coshedding flow for  $d/D=0.24$  and  $L/d=5.5$ . The difference could be attributed to a slightly higher turbulent intensity appearing in Alam and Zhou's measurement.

Depending on  $d/D$  and  $L/d$ , five scenarios are recognized, namely lock-in, intermittent lock-in, no lock-in, subharmonic lock-in and shear-layer reattachment. Their dependence on  $d/D$  and  $L/d$  can be illustrated in Fig. 8. The border between different regimes is identified with the midpoint between two adjacent measurement grid points where one scenario was found to change to another. The lock-in and reattachment regimes prevail at a small  $L/d$  ( $< 8$ ) with a large ( $> 0.9$ ) and a small ( $< 0.35$ )  $d/D$ , respectively (Fig. 8). When the  $d/D$  is large ( $> 0.9$ ) and  $L/d$  is small ( $< 8$ ), the gap vortices can trigger the vortex shedding from the DC, leading to a

**Fig. 8** Map of flow regimes in  $d/D$ - $L/d$  plane. **a**  $Re=0.8 \times 10^4$ , **b**  $Re=1.61 \times 10^4$  and **c**  $Re=2.42 \times 10^4$ . The symbols in figures denote the measurement points. Open square, reattachment regime; open revert triangle, no lock-in and intermittent lock-in regimes; filled triangle, subharmonic lock-in regime; filled square, lock-in regime



lock-in. An increase in  $L/d$  leads to an intermittent lock-in ( $5.5 < L/d < 12.5$ , depending on  $d/D$ ) followed by no lock-in ( $L/d > 12.5$ ). At  $L/d > 12.5$ , the gap vortices weaken before reaching the DC, failing to trigger the shedding from the DC. The  $St$ (s) of the two cylinders become different, no lock-in. As expected, the intermittent lock-in regime takes place at the border between lock-in and no lock-in regimes. The subharmonic lock-in regime appears at  $0.57 < d/D < 0.67$ ,  $L/d \geq 8$  for  $Re = 0.8 \times 10^4$  and  $1.61 \times 10^4$ , getting narrow and elongated for  $Re = 2.42 \times 10^4$ . The similarity in flow regimes between  $Re = 0.8 \times 10^4$  and  $1.61 \times 10^4$  might be connected to the fact that a single cylinder  $St$  is also less sensitive to  $Re$  in the range  $Re = 10^3$ – $10^4$  and more sensitive to  $Re$  for  $Re > 10^4$  (Zdravkovich 1997). As such, the vortex formation length of a single cylinder is about  $2.5D$  for  $Re = 10^3$ – $10^4$  and declines from  $2.5D$  to  $0.75D$  when  $Re$  is increased from  $10^4$  to  $4 \times 10^4$  (Zdravkovich 1997; Wang et al. 2017).

### 3.2 Strouhal number

The examination of the evolution of  $St$  of the two cylinders with  $L/d$  and  $d/D$  may provide a clearer picture of how the UC affects the DC vortex shedding frequency and vice versa. Figure 9 shows contour plots of  $St$ , as a function of  $L/d$  and  $d/D$ , of the UC (first row) and the DC (second row) at  $Re = 0.8 \times 10^4$ ,  $1.61 \times 10^4$  and  $2.42 \times 10^4$ . Let us first discuss  $St$  of the UC. The lowest  $St$  ( $\approx 0.20$ – $0.22$ ) is recorded in the lock-in and intermittent lock-in regimes. At a given  $L/d$  in no lock-in regime, the  $St$  augments with decreasing

$d/D$ , reaching about 0.85 at  $d/D = 0.25$ ,  $L/d > 10$ . The augmentation is higher for smaller  $d/D$ , in the regime below the subharmonic regime. The reattachment regime corresponds to a small  $St$  where the DC is within the vortex formation region of the UC and a cavity flow appears in the gap between the cylinders. With  $L/d$  increasing from the reattachment regime,  $St$  swells as the DC gets out of the UC cavity. In the subharmonic regime, the  $St$  is fairly constant,  $\approx 0.33$ . A contour line becomes approximately horizontal at  $L/d > 15$ , implying that the influence of the DC on the UC is insignificant, the UC essentially being an isolated cylinder.

For the DC (Fig. 9d–e), the scale in the color code bar is made different from that for the UC because the range of  $St$  is much smaller for the DC than for the UC. The  $St$  of the DC is smaller than that of an isolated cylinder except at the reattachment regime where  $St$  is almost equal to a single cylinder  $St$ . Even at the largest  $L/d = 20$  examined, the  $St$  is 10–25%, depending on  $d/D$ , smaller than that of an isolated cylinder. The observation suggests the DC flow is still substantially influenced by the UC. The lowest  $St$  prevails in intermittent lock-in regime. At a given  $L/d$ , the  $St$  enlarges with decreasing  $d/D$  as a decreased  $d/D$  yields less shielding and hence a greater velocity in the shear layer of the DC which will be discussed later. In the subharmonic lock-in regime,  $St$ , close to 0.165, is relatively less sensitive to  $L/d$  because the DC  $St$  is linked to the UC  $St$  ( $\approx 0.33$ , by a factor of 0.5) that does not vary much with  $L/d$  ( $> 10$ ) in the subharmonic lock-in regime.



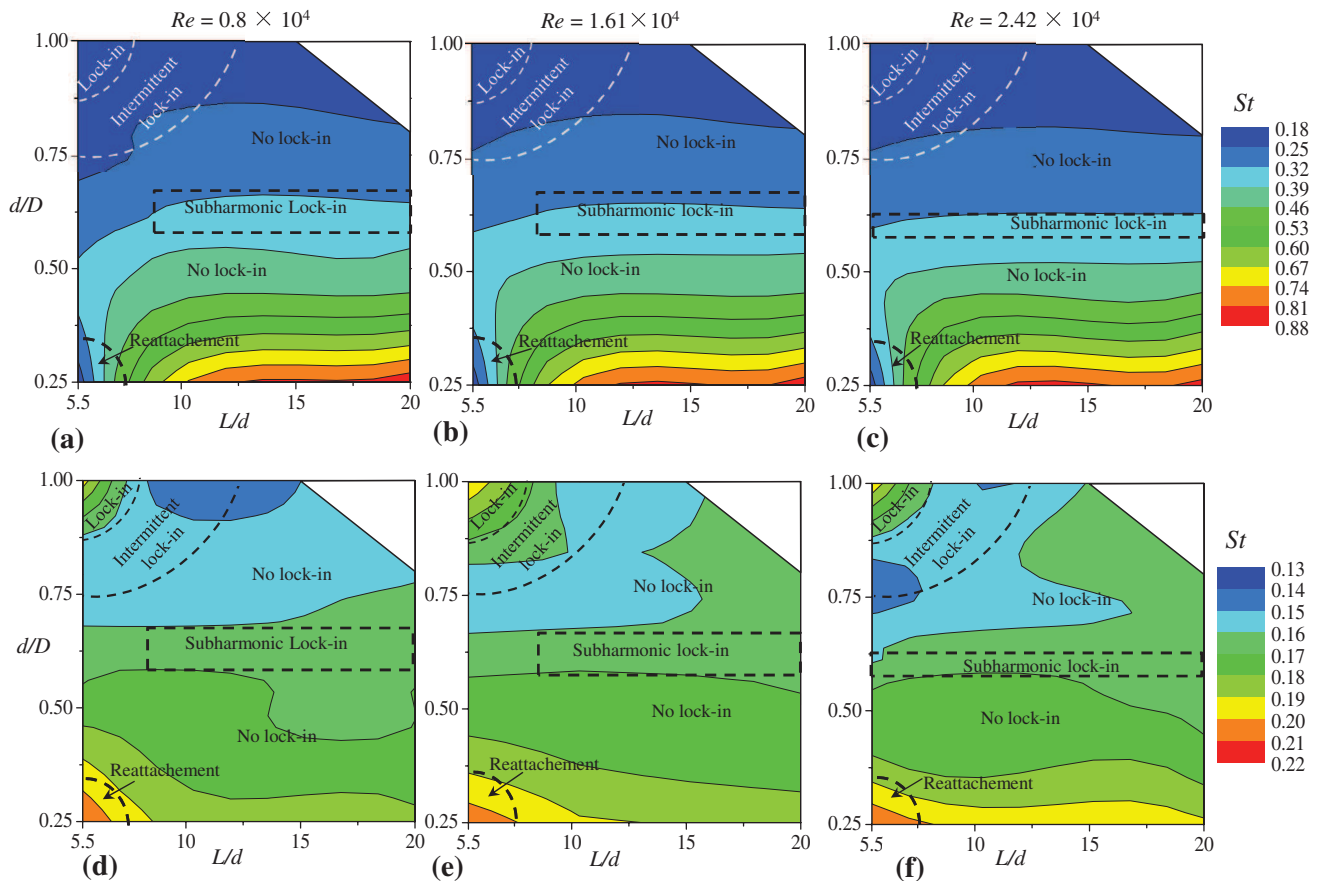


**Fig. 9** Contour plots showing the dependence on  $L/d$  and  $d/D$  of Strouhal number  $St$  of the upstream cylinder (first row) and downstream cylinder (second row). **a, d**  $Re=0.8 \times 10^4$ , **b, e**  $Re=1.61 \times 10^4$

and **c, f**  $Re=2.42 \times 10^4$ . Data for  $L/d=20$  and  $d/D=1.0$  were not measured, the upper right corner is, therefore, blank

### 3.3 Flow fields and wake

In the previous section, it is identified that both  $d/D$  and  $L/d$  albeit impact on  $St$ , the impact of  $d/D$  comes into being in a greater scale than that of  $L/d$ . It is thus worthy investigating how  $d/D$  influences the flow field. Contours of time-mean streamwise velocity  $\bar{u}^*(=u/U_\infty)$  are shown in Fig. 10 for the gap and the wake at  $Re=1.61 \times 10^4$ . Three different  $d/D=1.0, 0.6,$  and  $0.25$  at the same  $L/d=5.5$  are considered, corresponding to lock-in, no lock-in and reattachment regimes, respectively. This will explicate the information about the dependence of  $d/D$  on the flow field. On the other hand, to find the influence of  $L/d$  on the flow,  $L/d=10$  at  $d/D=0.6$  is chosen, lying in the subharmonic regime. A single cylinder flow field is also shown for a comparison purpose. The region enclosed by  $\bar{u}^*=0$  is called recirculation bubble.

Let us first examine the  $d/D$  effect. Obviously, the lateral width of the free shear layers in the gap narrows with decreasing  $d/D$ . The shear layer reattachment for  $d/D=0.25$  renders strong recirculation in the gap. The streamwise

length of the UC recirculation bubble elongates with  $d/D$  decreasing from 1.0 to 0.6 (Fig. 10a, b), explaining why the UC  $St$  boosts with decreasing  $d/D$ . For the DC, the bubble elongates from  $d/D=1.0$  to 0.6 (Fig. 10a, b) and shrinks from  $d/D=0.6$  to 0.25 (Fig. 10b, c). The velocity recovery rate differs significantly with  $d/D$ , a higher recovery occurring for a smaller  $d/D$ . This is due to a fact that a smaller UC renders a less shielding effect on UC. A comparison between Fig. 10b, d indicates that an increase in  $L/d$  (1) results in the recirculation shrinking for the DC, (2) a greater approaching flow in the gap, and (3) a higher velocity recovery in both gap and wake. The velocity recovery in the DC wake for any  $d/D$  is slower than that in the single cylinder wake, implying that the DC is yet substantially influenced by the UC.

The lateral width  $h^*(=h/D)$  between the two UC free shears (Fig. 10a–d) can be quantified as lateral separation between the two peaks in the profile of  $d\bar{u}^*/dy^*$  vs  $y^*$  at  $x^*=0.6$  (Roshko 1954; Balachandar et al. 1997). Figure 11a displays the dependence of  $h^*$  on  $d/D$ . The  $h^*$  varies linearly with  $d/D$ , a smaller  $d/D$  corresponding to a smaller  $h^*$ . This explains why the  $St$  of the UC increases with  $d/D$  decreasing



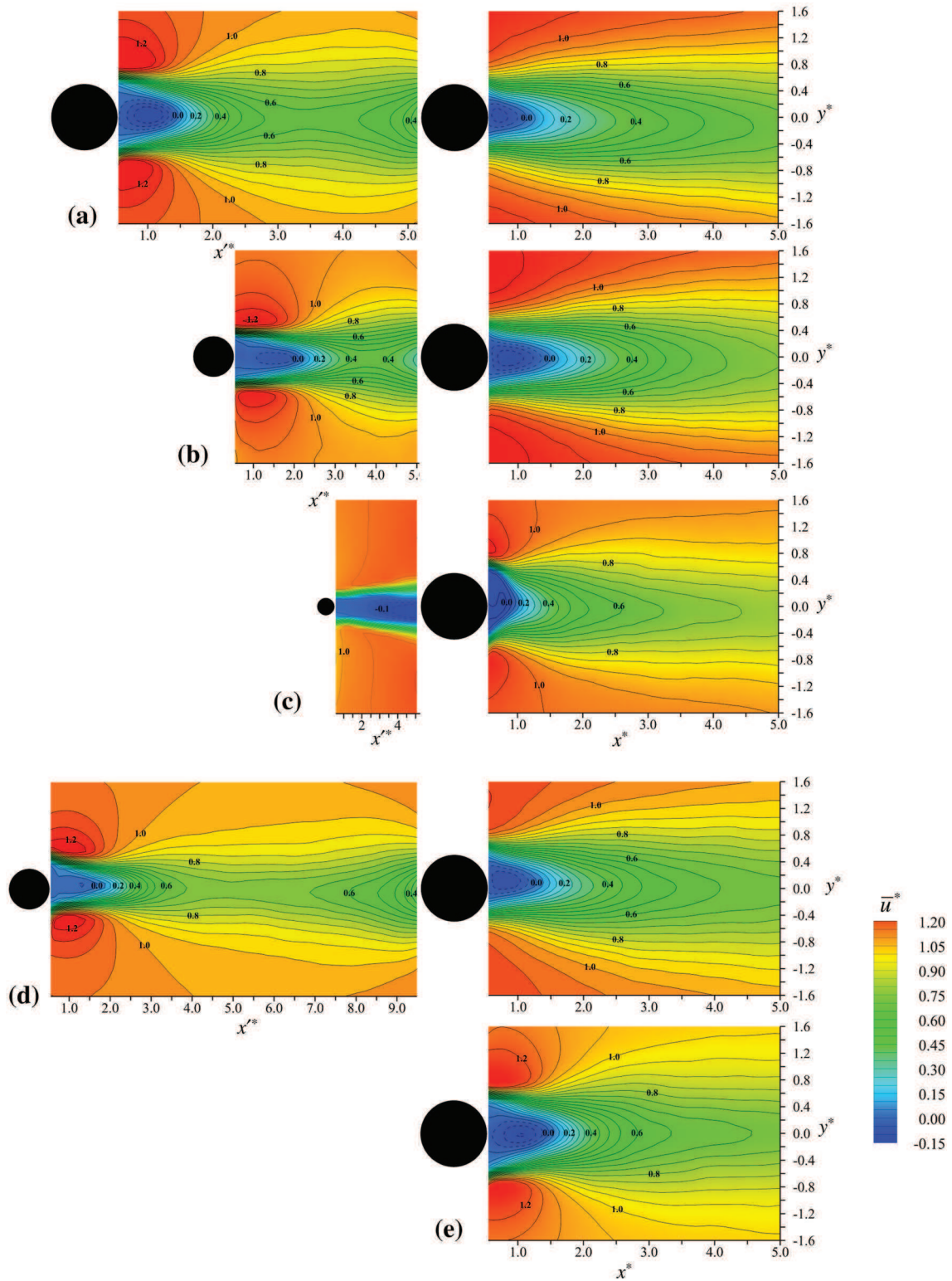


**Fig. 10** Contours of time-mean streamwise velocity  $u^*$  at  $Re=1.61 \times 10^4$ . **a**  $d/D=1.0$ ,  $L/d=5.5$ , **b**  $d/D=0.60$ ,  $L/d=5.5$ , **c**  $d/D=0.25$ ,  $L/d=5.5$ , **d**  $d/D=0.60$ ,  $L/d=10$ , and **e** single cylinder.

The solid and dashed lines represent positive ( $\geq 0$ ) and negative ( $< 0$ ) contour levels, respectively. The contour increment is 0.05

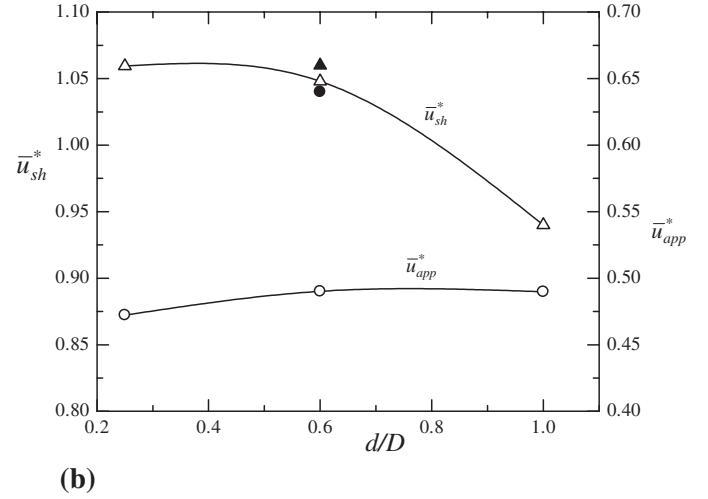
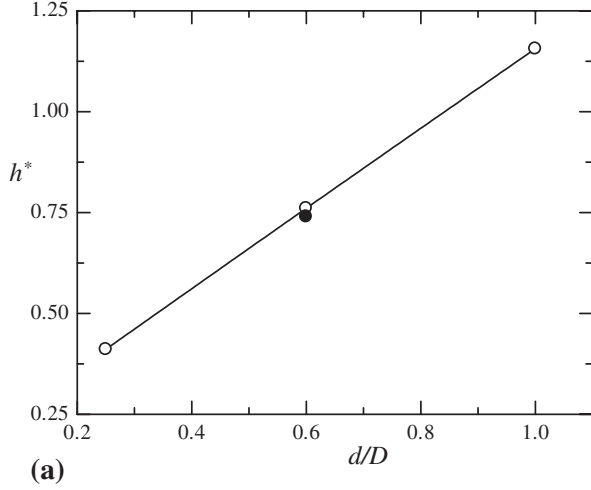


**Fig. 11** Dependence on  $d/D$  of **a** lateral distance  $h^*$  ( $=h/D$ ) between the upstream-cylinder free shear layers measured at  $x^* = 0.6$ , and **b** average approaching velocity  $\bar{u}_{app}^*$  over  $y^* = -0.5 \sim 0.5$  at  $x^* = -1.0$

and average shear layer velocity  $\bar{u}_{sh}^*$  over  $y^* = 0.5 \sim 1.5$  at  $x^* = 0.6$ . The open and solid symbols stand for  $L/d = 5.5$  and  $10$ , respectively.  $Re = 1.61 \times 10^4$

(Fig. 9). The change in  $L/d$  from  $5.5$  to  $10$  for  $d/D = 0.6$  does not lead to an appreciable departure. The  $h^*$  may also influence the flow around the DC, hence drag coefficient. The characteristics of the flow around the DC can be quantified as the averaged approaching flow velocity  $\bar{u}_{app}^*$  ( $= \int_{-0.5}^{0.5} \bar{u}^* dy^*$ ) measured at  $x^* = -0.6$  and the averaged shear layer velocity  $\bar{u}_{sh}^*$  ( $= \int_{0.5}^{1.5} \bar{u}^* dy^*$ ) measured at  $x^* = 0.6$ . The dependence of  $\bar{u}_{app}^*$  and  $\bar{u}_{sh}^*$  on  $d/D$  is presented in Fig. 11b. Interestingly,  $d/D$  has a profound effect on  $\bar{u}_{sh}^*$  but less on  $\bar{u}_{app}^*$ . The  $\bar{u}_{sh}^*$  boosts with decreasing  $d/D$ . On the contrary,  $L/d$  has a substantial influence on  $\bar{u}_{app}^*$  but not on  $\bar{u}_{sh}^*$  (compare the solid and open symbols),  $\bar{u}_{app}^*$  for  $d/D = 0.6$  increasing from  $0.49$  to  $0.64$  as  $L/d$  increases from  $5.5$  to  $10$ . Since  $\bar{u}_{sh}^*$  is largely connected to  $St$ , the invariance of  $\bar{u}_{sh}^*$  between  $L/d = 5.5$  and  $10$  for  $d/D = 0.6$  is consistent with that of  $St$ . Both  $\bar{u}_{app}^*$  and  $\bar{u}_{sh}^*$  may play a role in determining  $C_D$ , which will be discussed later.

Figure 12 shows fluctuating (r.m.s.) streamwise velocity  $u_{rms}^*$  ( $= u_{rms}/U_\infty$ ) for the same  $d/D$  and  $L/d$  as in Fig. 10. Two  $u_{rms}^*$  peaks behind each cylinder indicate the rolling positions of the shear layers. The lateral separation between the two peaks and their streamwise distance from the cylinder center are thus defined as the wake width and vortex formation length, respectively (Bloor 1964; Gerrard 1966; Griffin and Ramberg 1974; Roshko 1993). The maximum  $u_{rms}^*$  in the UC wake decays with decreasing  $d/D$  while an opposite scenario takes place in the DC wake (Fig. 12a–c). The small  $u_{rms}^*$  distributed along the shear layers in the gap (Fig. 12c) indicates the shear layer reattachment, absence of the alternating

vortex shedding from the UC. On the other hand, when  $L/d$  is increased for a given  $d/D$  (Fig. 12b, d), maximum  $u_{rms}^*$  increases for the DC but drops for the UC. The wake width and formation length of the UC, respectively, shrink and enlarge between  $d/D = 1.0$  and  $0.6$  (Fig. 12a, b), while the formation length of the DC grows between the same  $d/D$  and contracts between  $d/D = 0.6$  and  $0.25$  (Fig. 12b, c). When  $L/d$  is increased from  $5.5$  to  $10$ , the wake width dwindles and the formation length elongates, albeit a little, for the UC (Fig. 12b, d), both resulting in an increase in  $St$  (Fig. 6e) as a small wake width and/or a large formation length corresponds to a large  $St$  (Nakaguchi et al. 1968; Alam et al. 2011).

### 3.4 Forces on the downstream cylinder

It is expected that the forces on the DC are sensitive to  $d/D$  and  $L/d$ , while those on the UC are not much (Zhou and Alam 2016). Figure 13 shows variations in  $C_D$ ,  $C_D'$  and  $C_L'$  as a function of  $d/D$  and  $L/d$  at  $Re = 1.61 \times 10^4$ . A strong correlation between  $C_D$  and  $d/D$  or  $L/d$  is observed. For a given  $L/d$ ,  $C_D$  boosts with decreasing  $d/D$ . An increase in  $C_D$  also occurs when  $L/d$  is increased for a given  $d/D$ . That is, an increase in  $L/d$  or a decrease in  $d/D$  leads to an augmentation in  $C_D$ . How  $L/d$  and  $d/D$  influence the flow is, however, different from each other. A smaller  $d/D$  means a narrower  $h^*$  and a greater  $\bar{u}_{sh}^*$  (Fig. 11). The augmentation in  $C_D$  with decreasing  $d/D$  is thus caused by the increased  $\bar{u}_{sh}^*$  (Roshko 1954). The higher the  $\bar{u}_{sh}^*$  and/or  $\bar{u}_{app}^*$ , the larger the  $C_D$ . On the other hand, a longer  $L/d$  allows a greater  $\bar{u}_{app}^*$  (Fig. 11), which results in  $C_D$  increasing with  $L/d$ . At the largest  $L/d$

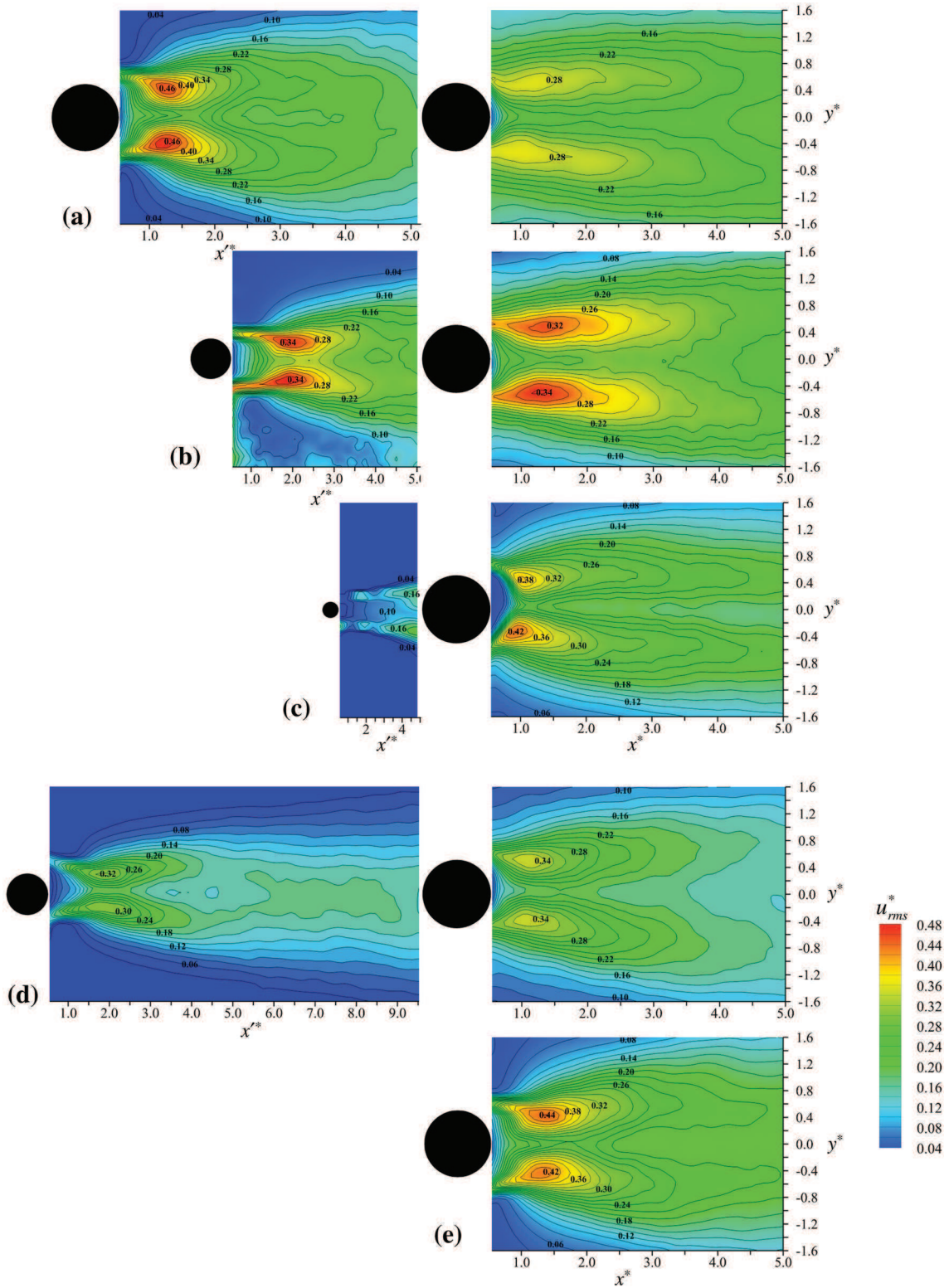
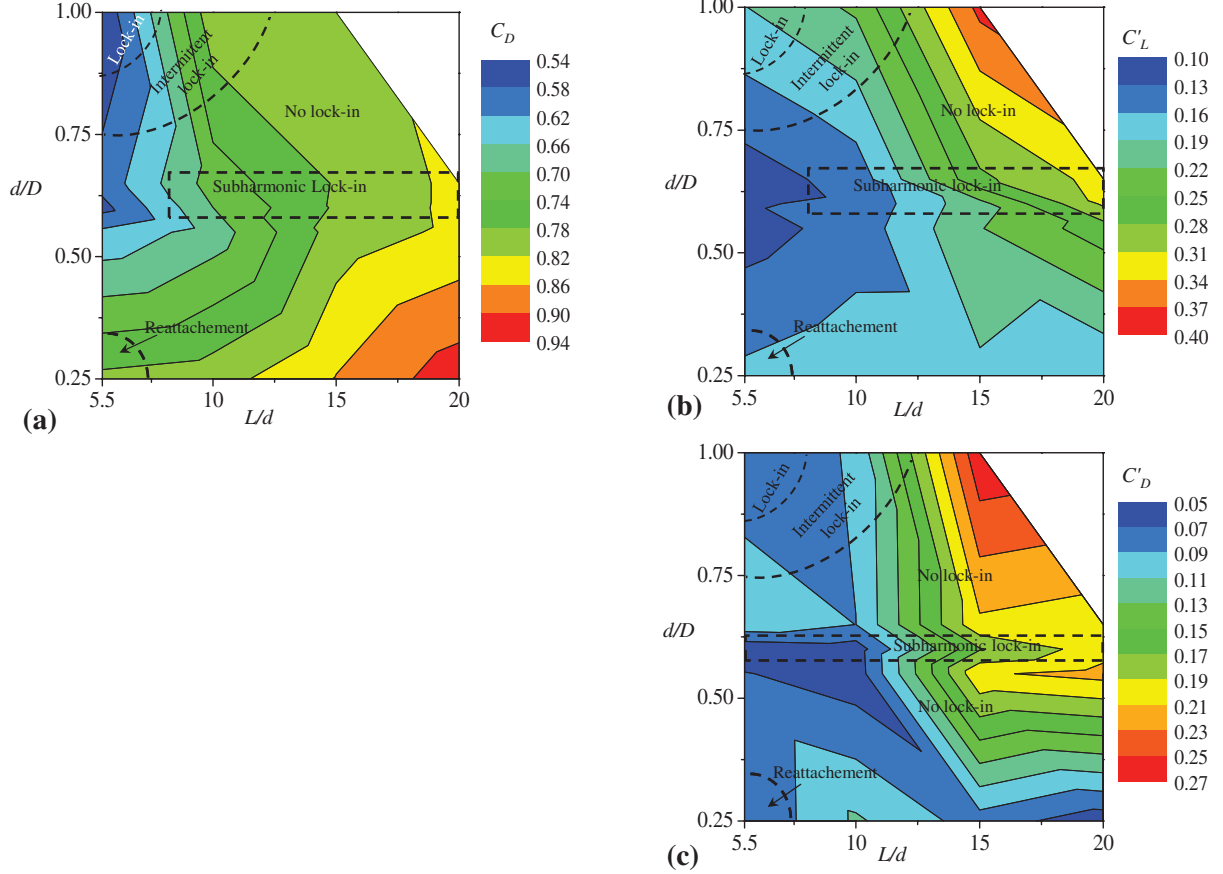


Fig. 12 Contours of fluctuating (r.m.s.) streamwise velocity  $u_{rms}^*$  at  $Re = 1.61 \times 10^4$ . **a**  $d/D = 1.0, L/d = 5.5$ , **b**  $d/D = 0.60, L/d = 5.5$ , **c**  $d/D = 0.25, L/d = 5.5$ , **d**  $d/D = 0.60, L/d = 10$ , and **e** single cylinder. The contour increment is 0.02



**Fig. 13** Dependence on  $L/d$  and  $d/D$  of the force coefficients of the downstream cylinder at  $Re = 1.61 \times 10^4$ . **a** Time-mean drag coefficient  $C_D$ , **b** fluctuating lift coefficient  $C'_L$ , **c** fluctuating drag coefficient  $C'_D$ .

(=20) and smallest  $d/D$  (=0.25) examined,  $C_D$  is the largest (=0.92), but still smaller by 17%, compared to that of an isolated cylinder ( $C_D = 1.11$ ). Oppositely, the lowest  $C_D$  (=0.55) occurs at  $d/D = 1$ ,  $L/d = 5.5$ . A relatively large increase in  $C_D$  is observed for  $d/D = 1.0$  between  $L/d = 5.5$  and 10, concomitant with the change in lock-in to no lock-in. Interestingly, the recovery of  $C_D$  with increasing  $L/d$  is smaller for  $d/D \approx 0.6-0.65$ , corresponding to the subharmonic lock-in.

In general,  $C'_D$  and  $C'_L$  increase with  $L/d$ , albeit rather rapidly for  $L/d \geq 10$ , particularly for  $d/D > 0.5$ . The increase is largely due to the DC vortex shedding enhancing with  $L/d$ , consistent with the associated peak heightening with  $L/d$  (Fig. 5). The  $\bar{u}_{app}^*$  essentially contributes to strengthening the vortex shedding (Fig. 11). On the other hand,  $C'_D$  and  $C'_L$  both decline with decreasing  $d/D$  because of a weaker impingement of small vortices shed from the smaller diameter cylinder. Table 3 displays numerical data of  $C_D$ ,  $C'_D$  and  $C'_L$ , and a comparison is made incorporating data from Igarashi (1981), Kitagawa and Ohta (2008) and Cooper (1974) for

Data for  $L/d = 20$  and  $d/D = 1.0$  were not measured, the upper right corner is, therefore, blank

similar configurations and  $Re$ . For  $d/D = 1.0$ , the present  $C_D$  at  $L/d = 15$  agrees with that at  $L/d = 19.7$  by Cooper (1974), given that the effect of  $L/d$  on  $C_D$  is small for  $L/d > 10$ . Igarashi's (1981) and Kitagawa and Ohta's (2008)  $C_D$  at  $L/d = 4.5$  are overestimated and underestimated, respectively, compared to the present  $C_D$  at  $L/d = 5.5$ .

## 4 Conclusions

We examined the influence of the diameter ratio  $d/D$  (=0.25–1.0), spacing ratio  $L/d$  (=5.5–20) and Reynolds number  $Re$  ( $=0.8 \times 10^4 - 2.42 \times 10^4$ ) on the flow structure, Strouhal number  $St$  and forces. The other parameters investigated are power spectral density functions, time-mean streamwise velocity  $\bar{u}^*$ , fluctuating (r.m.s.), streamwise velocity  $u_{rms}^*$ , the lateral distance  $h^*$  between the UC free shear layers, average approaching velocity  $\bar{u}_{app}^*$ , and average shear layer velocity  $\bar{u}_{sh}^*$ . The investigation leads to the following conclusions.



**Table 3** The values of  $C_D$ ,  $C'_D$  and  $C'_L$  at different  $d/D$  and  $L/d$ .  $Re = 1.61 \times 10^4$

$d/D$	$L/D$	$C_D$	$C'_D$	$C'_L$
0.25	5.5	0.790	0.070	0.120
	10	0.802	0.113	0.179
	15	0.862	0.080	0.183
	20	0.923	0.058	0.140
0.55	5.5	0.629	0.071	0.116
	10	0.678	0.058	0.142
	15	0.798	0.207	0.219
	20	0.829	0.217	0.266
0.60	5.5	0.567	0.055	0.127
	10	0.700	0.060	0.136
	15	0.785	0.168	0.211
	20	0.831	0.201	0.315
0.65	5.5	0.595	0.104	0.114
	10	0.718	0.090	0.142
	15	0.783	0.206	0.273
	20	0.831	0.198	0.322
1.0	5.5	0.544	0.076	0.189
		0.58 (Igarashi 1981, $L/d=4.5$ , $Re=2.1 \times 10^4$ )		
		0.52 (Kitagawa and Ohta 2008, $L/d=4.5$ , $Re=2.2 \times 10^4$ )		
	10	0.780	0.092	0.225
	15	0.802	0.267	0.379
	0.8 (Cooper 1974, $L/d=19.7$ , $Re=2.24 \times 10^4$ )			

The flow around the cylinders depends on both  $d/D$  and  $L/d$ , classified into five regimes, namely lock-in, intermittent lock-in, no lock-in, subharmonic lock-in and shear-layer reattachment regimes. While the lock-in regime occurs at large  $d/D > 0.9$ , the reattachment regime takes place at small  $d/D < 0.35$ , both for small  $L/d < 8$ . The former regime is characterized by the DC vortex shedding triggered by the UC. On the other hand, the latter features reattachment of the UC shear layers on the DC. The  $St$  of a cylinder is thus identical to that of the other for both regimes. The intermittent lock-in regime ( $5.5-8 < L/d < 12.5$ ,  $0.7-0.9 < d/D < 1.0$ ) prevails between the lock-in and no lock-in regimes, characterized by two  $St$  for the DC and one  $St$  for the UC. In the no lock-in regime ( $L/d > 5.5-12.5$ , depending on  $d/D$ ), the  $St$  of the DC differs from that of the UC,  $St$  being larger for the UC than for the DC. The subharmonic lock-in regime appears at  $0.57 < d/D < 0.67$ ,  $L/d > 8$  for  $Re = 0.8 \times 10^4$  and  $1.61 \times 10^4$ , getting narrow and elongated for  $Re = 2.42 \times 10^4$ . The value of the DC  $St$  is half that of the UC.

At a given  $L/d$ , the  $St$  of the UC swells with decreasing  $d/D$ , from  $St = 0.2$  to  $0.85$  when  $d/D$  decreasing from  $1.0$  to

$0.25$  ( $L/d > 10$ ). The swelling is attributed to a smaller  $h^*$  for a smaller  $d/D$ . While the smallest  $St$  for the UC appears in the lock-in regime, the largest  $St$  for the DC prevails for reattachment regime. With  $L/d$  increasing from the reattachment regime, the  $St$  contracts for the DC but enhances for the UC. The enhancement is accompanied by a small wake width and/or a large formation length. In general, at a given  $L/d$ , the  $St$  of DC grows with decreasing  $d/D$ , caused by the increased  $\bar{u}_{sh}^*$ . The  $St$  of the DC at the largest  $L/d = 20$  examined is 10–25%, depending on  $d/D$ , smaller than that of an isolated cylinder, the DC flow being yet substantially influenced by the UC.

Following  $St$ , forces are also highly dependent on  $L/d$  and  $d/D$ . A decrease in  $d/D$  or an increase  $L/d$  yields a rise in  $C_D$ . While the rise in  $C_D$  with decreasing  $d/D$  results from the increased  $\bar{u}_{sh}^*$ , that with increasing  $L/d$  is caused by a greater  $\bar{u}_{app}^*$ . The lowest value of the  $C_D$  ( $=0.55$ ) appears at  $d/D = 1.0$ ,  $L/d = 5.5$  while the largest value of  $C_D$  ( $=0.92$ ) emerges at  $d/D = 0.25$ ,  $L/d = 20$ , still smaller by 17%, compared to that of an isolated cylinder ( $C_D = 1.11$ ). In general, an increase in  $L/d$  goes with  $C'_D$  and  $C'_L$  increasing, rather rapidly for  $L/d > 10$ ,  $d/D > 0.5$ . An increased  $\bar{u}_{app}^*$  essentially contributes to the increased  $C'_D$  and  $C'_L$ . A decrease in  $d/D$  results in  $C'_D$  and  $C'_L$  both declining because of the generation of smaller vortices from the smaller diameter cylinder.

**Acknowledgements** Alam wishes to acknowledge the support given by the National Natural Science Foundation of China through Grants 11672096 and 91752112.

## References

- Alam MM (2014) The aerodynamics of a cylinder submerged in the wake of another. *J Fluids Struct* 51:393–400
- Alam MM (2016) Lift forces induced by the phase lag between the vortex sheddings from two tandem bluff bodies. *J Fluids Struct* 65:217–237
- Alam MM, Sakamoto H (2005) Investigation of Strouhal frequencies of two staggered bluff bodies and detection of multistable flow by wavelets. *J Fluids Struct* 20(3):425–449
- Alam MM, Zhou Y (2007) The turbulent wake of an inclined cylinder with water running. *J Fluid Mech* 589:261–303
- Alam MM, Zhou Y (2008) Strouhal numbers, forces and flow structures around two tandem cylinders of different diameters. *J Fluids Struct* 24(4):505–526
- Alam MM, Moriya M, Takai K, Sakamoto H (2003) Fluctuating fluid forces acting on two circular cylinders in a tandem arrangement at a subcritical Reynolds number. *J Wind Eng Ind Aerodyn* 91(1):139–154
- Alam MM, Zhou Y, Zhao JM, Flamand O, Buojar O (2010) Classification of the tripped cylinder wake and bi-stable phenomenon. *Int J Heat Fluid Flow* 31:545–560
- Alam MM, Zhou Y, Wang XW (2011) The wake of two side-by-side square cylinders. *J Fluid Mech* 669:432–471



- Assi GRS, Bearman PW, Meneghini JR (2010) On the wake-induced vibration of tandem circular cylinders: the vortex interaction excitation mechanism. *J Fluid Mech* 661:365–401
- Balachandar S, Mittal R, Najjar FM (1997) Properties of the mean recirculation region in the wakes of two-dimensional bluff bodies. *J Fluid Mech* 351:167–199
- Barnes FH, Grant I (1983) Vortex shedding in unsteady flow. *J Wind Eng Ind Aerodyn* 11(1):335–344
- Baxendale AJ, Grant I, Barnes FH (1986) Vortex shedding from two cylinders of different diameters. *J Wind Eng Ind Aerodyn* 23(1–3):427–435
- Bloor MS (1964) The transition to turbulence in the wake of a circular cylinder. *J Fluid Mech* 19:290–304
- Cooper KR (1974) Wind tunnel measurements of the steady aerodynamics forces on a smooth circular cylinder immersed in the wake of an identical cylinder. National Research Council of Canada LTR-LA-119
- Gerrard JH (1966) The mechanics of the formation region of vortices behind bluff bodies. *J Fluid Mech* 25:401–413
- Griffin OM, Ramberg SE (1974) The vortex street wakes of vibrating cylinders. *J Fluid Mech* 66:553–576
- Hiwada M, Taguchi T, Mabuichi I, Kumada M (1979) Fluid flow and heat transfer around two circular cylinders of different diameters in cross flow. *Bull JSME* 22:715–723
- Igarashi T (1981) Characteristics of the flow around two circular cylinders arranged in tandem (1st report). *Bull JSME* 24:323–331
- Igarashi T (1982) Characteristics of the flow around two circular cylinders of different diameters arranged in tandem. *Bull JSME* 25(201):349–357
- Igarashi T (1984) Characteristics of the flow around two circular cylinders arranged in tandem (2nd report). *Bull JSME* 27: 2380–2387
- Kitagawa T, Ohta H (2008) Numerical investigation on flow around circular cylinders in tandem arrangement at a subcritical Reynolds number. *J Fluids Struct* 24:680–699
- Konstantinidis E, Balabani S (2008) Flow structure in the locked-on wake of a circular cylinder in pulsating flow: Effect of forcing amplitude. *Int J Heat Fluid Flow* 29(6):1567–1576
- Konstantinidis E, Balabani S, Yianneskis M (2003) The effect of flow perturbations on the near wake characteristics of a circular cylinder. *J Fluids Struct* 18(3–4):367–386
- Lau YL, So RMC, Leung RCK (2004) Flow-induced vibration of elastic slender structures in a cylinder wake. *J Fluid Struct* 19:1061–1083
- Lee SJ, Lee SI, Park CW (2004) Reducing the drag on a circular cylinder by upstream installation of a small control rod. *Fluid Dyn Res* 34(4):233–250
- Lesage F, Gartshore IS (1987) A method of reducing drag and fluctuating side force on bluff bodies. *J Wind Eng Ind Aerodyn* 25(2):229–245
- Mahír N, Altac Z (2008) Numerical investigation of convective heat transfer in unsteady flow past two cylinders in tandem arrangements. *Int J Heat Fluid Flow* 29:1309–1318
- Mavridou SG, Bouris DG (2012) Numerical evaluation of a heat exchanger with inline tubes of different size for reduced fouling rates. *Int J Heat Mass Transf* 55:5185–5195
- Nakaguchi H, Hashimoto K, Muto S (1968) An experimental study on aerodynamic drag of rectangular cylinder. *J Jpan Soc Aeronaut Space Sci* 16(168):1–5
- Norberg C (1994) An experimental investigation of the flow around a circular cylinder: influence of aspect ratio. *J Fluid Mech* 258:287–316
- Prasad A, Williamson CHK (1997) A method for the reduction of bluff body drag. *J Wind Eng Ind Aerodyn* 69–71(4):155–167
- Qin B, Alam MM, Zhou Y (2017) Two tandem cylinders of different diameters in crossflow: flow-induced vibration. *J Fluid Mech* 829:621–658
- Roshko A (1954) On the drag and shedding frequency of two-dimensional bluff bodies. NACA Tech. Note No. 3169
- Roshko A (1993) Perspectives on bluff body aerodynamics. *J Wind Eng Ind Aerodyn* 49(1):79–100
- Sakamoto H, Haniu H (1988) Aerodynamic forces acting on two square prisms placed vertically in a turbulent boundary layer. *J Wind Eng Ind Aerodyn* 31:41–66
- Sumner D (2010) Two circular cylinders in cross-flow: A review. *J Fluids Struct* 26(6):849–899
- Wang LJ, Alam MM, Zhou Y (2017) Two tandem cylinders of different diameters in crossflow: effect of an upstream cylinder on wake dynamics. *J Fluid Mech* 836:5–42
- West GS, Apelt CJ (1993) Measurements of fluctuating pressures and forces on a circular cylinder in the Reynolds number range  $10^4$  to  $2.5 \times 10^5$ . *J Fluids Struct* 7(3):227–244
- West GS, Apelt CJ (1997) Fluctuating lift and drag forces on finite lengths of a circular cylinder in the supercritical Reynolds number range. *J Fluids Struct* 11(11):135–158
- Zdravkovich MM (1977) Review of flow interference between two circular cylinders in various arrangements. *J Fluids Eng* 99(4):618–663
- Zdravkovich MM (1997) Flow around circular cylinders: fundamentals. Oxford science publications, Oxford
- Zhao M, Cheng L, Teng B, Liang D (2005) Numerical simulation of viscous flow past two circular cylinders of different diameters. *Appl Ocean Res* 27:39–55
- Zhou Y, Alam MM (2016) Wake of two interacting circular cylinders: A review. *Int J Heat Fluid Flow* 62:510–537